# A scalable, Rotating Disc Bioelectrochemical Reactor (RDBER) suitable for the cultivation of both cathodic and anodic biofilms

*Max Hackbarth [a], Johannes Gescher [b, c, d], Harald Horn [a, e], Johannes Eberhard Reiner [a,*].*

[a] Engler-Bunte-Institut, Water Chemistry and Water Technology, Karlsruhe Institute of Technology (KIT), Engler-Bunte-Ring 9a, 76131 Karlsruhe, Germany

[b] Karlsruhe Institute of Technology (KIT), Institute for Applied Biosciences (IAB), Fritz-Haber-Weg 2, 76131, Karlsruhe, Germany

[c] Karlsruhe Institute of Technology (KIT), Institute for Biological Interfaces (IBG 1), Hermann-von-Helmholtz-Platz 1, 76344 Eggenstein-Leopoldshafen, Germany

[d] Hamburg University of Technology, Institute of Technical Microbiology, Kasernenstraße 12, 21073 Hamburg, Germany

[e] DVGW Research Centre, Water Chemistry and Water Technology, Engler-Bunte-Ring 9a, 76131 Karlsruhe, Germany

** Address correspondence to Johannes Eberhard Reiner, reiner@kit.edu, + 49 721 608 – 4 789 3*

**Abstract**

This study presents the construction and operation of a membrane-less reactor suitable for different bioelectrochemical applications. The system employs rotating graphite disks as working electrodes with a total surface area of 1 $m^2$. Given the reactor volume of 10 L, this results in a surface-to-volume ratio of 100:1 $m^2$ $m^{-3}$. Moreover, this rotating disk bioelectrochemical reactor (RDBER) is fully autoclavable, pressurizable to at least 0.5 bars and an optical window allows for in vivo monitoring of biofilm development on the electrodes by means of optical coherence tomography (OCT). As a proof-of-principle for an aerobic microbial electrosynthesis process, we cultivated the thermoacidophilic, electroautotrophic bacterium *Kyrpidia spormannii* in the RDBER and investigated the spatial distribution of the cathodic biofilm on the rotating working electrode by OCT. Thereby, biofilm heights of more than 75 µm were achieved. To demonstrate the versatility of the system, we further operated the reactor anodically as a microbial electrolysis cell employing a co-culture of *Shewanella oneidensis* and *Geobacter sulfurreducens*. Finally, the cultivation experiments with different electroactive microorganisms not only prove the basic functionality of the RDBER, but also illustrate that the RDBER can satisfy a wide range of biotechnological requirements for pure culture applications.

## Graphical Abstract

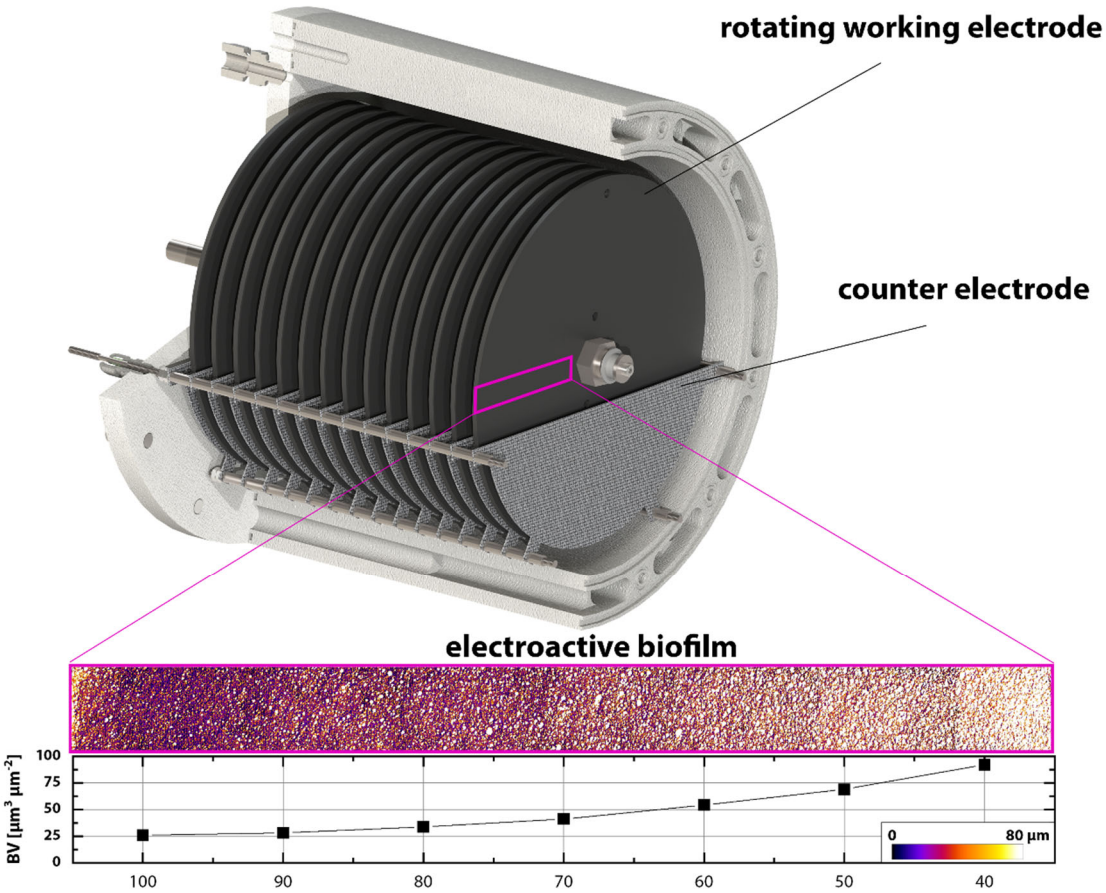


## Highlights

- **Construction of a 10 L membrane-less, pressurizable bioelectrochemical reactor**
- **Rotating working electrodes with up to 1 m$^2$ electrode surface**
- **Electroautotrophic cultivation and quantification of *K. spormannii* biofilms**
- **Initial cell density crucial for successful *K. spormannii* biofilm formation**
- **Anodic operation as MEC with *Shewanella* / *Geobacter* coculture**

**Keywords**

microbial electrosynthesis; microbial electrolysis cell; Kyrpidia spormannii; RDBER; RBC; microbial electrochemical technologies; pure culture MES upscaling;

## 1. Introduction

Tapering off fossil resources by renewable commodities that are based on a circular utilization of resources is key to the transition towards a sustainable economy (Lieder and Rashid, 2016). In this context, future (bio)chemical transformations of raw materials and waste streams must be fueled by renewable electrical energy (Krieg et al., 2018b). The so-called microbial electrosynthesis (MES) is a promising biotechnological example for such a conversion of electricity and carbon dioxide into value-added organic compounds (Nevin et al., 2010). This process relies on electroactive microorganisms that serve as a biocatalyst on the cathode of a bioelectrochemical system (BES) (Logan et al., 2019). By applying a voltage to the BES, typically water is oxidized at the anode into oxygen and protons. Driven by a power source the released electrons are subsequently used either directly or indirectly by the autotrophic, cathodic biofilm as the sole energy and electron source for the reduction of $CO_2$. Although MES could theoretically outperform abiotic carbon utilization technologies as well as established gas fermentations in some specific applications, the technology is not yet economically feasible on a large scale (Christodoulou and Velasquez-Orta, 2016; Jourdin et al., 2020; Jourdin and Burdyny, 2021; Prévoteau et al., 2020; Wood et al., 2021). However, the novel electroautotrophic species *Kyrpidia spormannii* EA-1$^T$ was isolated from a thermophilic cathodic community recently (Reiner et al., 2018a, 2018b). This thermoacidophilic 'Knallgas' bacterium is a natural producer of polyhydroxyalkanoates (PHAs) and was shown to thrive on cathodes as the sole electron and energy source for the reduction of $CO_2$ (Reiner et al., 2020). Hence, *K. spormannii* is a promising candidate for MES - not only since PHAs are precursors for biodegradable bioplastics - but also due to the organisms comparably good biofilm-formation abilities on cathodes. Thus, it was shown that *K. spormannii* forms robust biofilms with a thickness of well over 100 µm – an important prerequisite for MES as stated recently by Vassilev and colleagues (Barham et al., 1984; Hackbarth et al., 2020; Vassilev et al., 2022). Although it seems to be an intrinsic property of electroautotrophic organisms, the

88 molecular details of extracellular electron uptake (EET) from a cathode are also subject to keen
89 debate with regard to *K. spormannii* (Jung et al., 2020; Pillot et al., 2022a; Prévoteau et al.,
90 2020; Reiner et al., 2020).

91 While - with respect to the inanimate components of a MES system - much effort has been put
92 into studying the effect of material and structural properties of electrodes, the development of
93 new and, in particular, scalable reactor concepts for MES has been rather sidelined (Enzmann
94 et al., 2018; Guo et al., 2015; Kerzenmacher, 2017; Pillot et al., 2022a, 2022b; Zhang et al.,
95 2021). This is in spite of the fact that whether microbial electrochemical technologies (METs)
96 can carve a niche in a future sustainable economy depends strongly on the availability of a
97 suitable reactor technology. Typical reactor systems for the cultivation of electroactive
98 microorganisms in laboratory settings are cube, bottle, or flat-plate-type reactors (Enzmann et
99 al., 2019; Krieg et al., 2018a). Especially for MES applications, a semipermeable membrane
100 is commonly required to spatially separate anode and cathode compartments. Membranes can
101 be advantageous when extremely high Coulombic efficiencies are desired, as they avoid
102 chemical short circuits caused by diffusion of electrochemically active chemicals (Krieg et al.,
103 2018a). Moreover, due to anodically produced oxygen a membrane is particularly crucial if
104 strict anaerobes, such as acetogenic or methanogenic organisms, serve as cathodic
105 biocatalysts for MES (Gildemyn et al., 2017). However, the utilization of membranes leads to
106 significantly increased surface-specific ohmic losses as a plain result of an increased distance
107 between anode and cathode, but also through diffusion limitations often caused by hardly
108 mixed zones around the membranes. The latter may also result in undesirable pH shifts in the
109 separated compartments (Gildemyn et al., 2017; Guo et al., 2017; Krieg et al., 2018a;
110 Prévoteau et al., 2020; Zeppilli et al., 2016). Finally, most membranes are not autoclavable
111 (according to the manufacturer), sensitive to fouling and prone to leakage due to lack of
112 mechanical stability (Utesch and Zeng, 2018). The above-mentioned disadvantages of
113 membranes, along with the resulting complexity of the reactor set-up, lead to a high-
114 maintenance reactor system which is likely to be very cost-intensive in long-term operation
115 (Kracke et al., 2018).

116 Here, we present the concept of a membrane-less, scalable rotating disk bioelectrochemical
117 reactor (RDBER) for aerobic MES and other pure culture bioelectrochemical applications. The
118 systems design is inspired by a so-called rotating biological contactor (RBC) (Hassard et al.,
119 2015). An RBC is a fixed-film bioreactor used in wastewater treatment that consists of closely
120 spaced discs that are mounted on a common horizontal shaft and are typically partially
121 submerged in liquid. Cortez and colleagues highlight the low maintenance and operating costs,
122 ease of process control and monitoring, and low land requirements as particular advantages
123 of an RBC (Cortez et al., 2008). This is mainly due to the fact that the flow velocity across the
124 biofilm enhancing substrate supply is not achieved by energy-intensive pumping of high
125 volumes or stirring, but by rotation of the biofilm-covered disks. The first steps in the
126 "electrification" of RBCs have already been successfully carried out on a laboratory scale
127 (Cheng et al., 2012, 2011; Rodziewicz et al., 2019; Sayess et al., 2013): Several attempts have
128 been made to use conductive rotating disks as cathode or anode of a bioelectrochemical
129 system. However, these studies consistently focus on the purification of wastewater. Hence,
130 biotechnological requirements for a pure culture MES process (e.g., working with pure cultures
131 under sterile conditions, control of temperature and pH, or pressurizability to increase the
132 solubility of the gaseous substrates like $CO_2$) were not considered in the reactor design.

133 In this study we discuss the development of a fully autoclavable RDBER, that can be
134 pressurized to at least 0.5 bar, and is equipped with an optical window allowing for in vivo
135 monitoring of biofilm development on the electrodes using optical coherence tomography
136 (OCT). The 10-liter membrane-less system operates in either anodic (as a microbial
137 electrolysis cell) or cathodic mode with an effective working electrode area of up to 1 $m^2$
138 (depending on the number of graphite disks mounted). As a proof of principle for an axenic,
139 aerobic MES-process we cultivated *K. spormannii* in the system and correlated the OCT-
140 derived, spacial resolved biovolume of the cathodic biofilm with the radius of the rotating
141 cathodes. Furthermore, we demonstrated that the developed system can also be operated as
142 a microbial electrolysis cell by culturing a co-culture of *Shewanella oneidensis* and *Geobacter*
143 *sulfurreducens* as an anodic biofilm in the RDBER. Thus, we were not only able to demonstrate

144 the general functionality of the system, but also to provide a first insight into the range of
145 possible applications that the RDBER offers as a technological platform for METs.

146

147 ## 2. Material and methods

148 ### 2.1 Reactor Design

149 The design of the reactor system is illustrated in detail in Fig. 1. The reaction chamber,
150 consisting of the reactor jacket (Fig. 1b) and two flanges, was designed as a horizontal cylinder
151 made of polypropylene. The inner diameter of the jacket measuring 238 mm and the length of
152 230 mm result in an inner volume of the reaction chamber of 10 L. An inspection window made
153 of polycarbonate (Fig. 1a) was integrated in the front flange allowing the observation of the
154 foremost working electrode (Fig. 1d). A circular recess milled in the center of the window serves
155 as a guide and seat for the shaft bearing (Fig. 1f). Figure 1 III shows a cross-sectional view of
156 the RDBER illustrating the arrangement of the electrodes in the reaction chamber. The shaft,
157 which was made of high-purity titanium and sealed from the environment by a shaft seal, is
158 located concentrically in the reactor. A precisely aligned shaft bearing in the rear flange,
159 together with the fixed bearing in the front window, ensures that the shaft runs as friction-free
160 and balanced as possible. For compensation of the temperature-related expansion of the shaft
161 relative to the reaction chamber, the bearing in the rear flange was designed as a floating
162 bearing. The shaft was manufactured as a threaded rod onto which working electrode holders
163 (custom made titanium nuts) are mounted. The working electrode discs made of graphite are
164 clamped between two holders in each case and centered in the process. This ensures that the
165 discs are in contact with the shaft and thus also with the voltage source. In total, up to 14
166 working electrode disks with a thickness of 3 mm and a diameter of 210 mm can be mounted
167 on the shaft. This corresponds to an active working electrode surface (front and back) of up to
168 1 $m^2$ and, relative to the reaction chamber volume, a surface-to-volume ratio of 100 $m^2$ $m^{-3}$.

169 Since in RBC-like systems the cross-flow across the biofilm is adjusted by the rotational speed
170 of the rotating substrate (here the working electrode), a high-resolution stepper motor (Fig. 1c)

171 was implemented (Lexium MDrive Motion Control, Schneider Electric) on the rear flange. The
172 employment of such a stepper motor allows, in addition to the load-independent control of the
173 rotational speed, the position-accurate visualization of selected locations on the substrate.
174 Apart from the toothed belt wheel required for this purpose, a double leg carbon brush holder
175 (Fig. 1l) with silver-graphite brushes was attached to the end of the titanium shaft (Fig. 1n). Via
176 this brush holder, electrical contact was made from the potentiostat to the rotating shaft and
177 thus also to the working electrodes. The counter electrodes were made of titanium sheet with
178 an iridium mixed oxide coating (platinode type 177, Umicore) in the form of half-rounds (Fig.
179 1m) and connected to each other by means of four titanium threaded rods (Fig. 1o). Exactly
180 cut pieces of titanium pipe (Fig. 1p) are mounted between each two anode sheets to provide
181 the desired distance between the working and counter electrodes. The distance between
182 anode and cathode amount to 5.5 mm. A total of up to 15 fixed counter electrode sheets with
183 an active area of approx. 0.5 m² can be installed in the reaction chamber in this way. The four
184 titanium threaded rods are led out of the reaction chamber through the rear flange (Fig. 1i) and
185 can thus be connected to the potentiostat. Cable bushings made of polytetrafluoroethylene
186 (PTFE) provide the necessary sealing.

187 In order to supply the growing biofilm with $CO_2$-enriched media during cathodic operation, the
188 gas-saturated and pre-tempered culture medium was pumped by means of a gear pump with
189 an autoclavable pump head (REGLO-Z Digital, Z-1830 P, Ismatec) (Fig. 1t) from an optional
190 stainless-steel (Fig. 1r) double jacket container via a compression fitting (Fig. 1e) located in
191 the front flange into the reaction chamber. The medium is then circulated in the overall system
192 via two screw fittings (Fig. 1h, j) located on the rear flange. During operation the volume flow
193 was led via the compression fitting (Fig. 1j) connected to the reference electrode holder
194 containing an Ag/AgCl reference electrode (Fig. 1q) (SE23I, Meinsberg Sensortechnik). The
195 second screw connection (Fig. 1h) served as an outlet for any gas that may have formed and
196 collected in the reaction chamber.

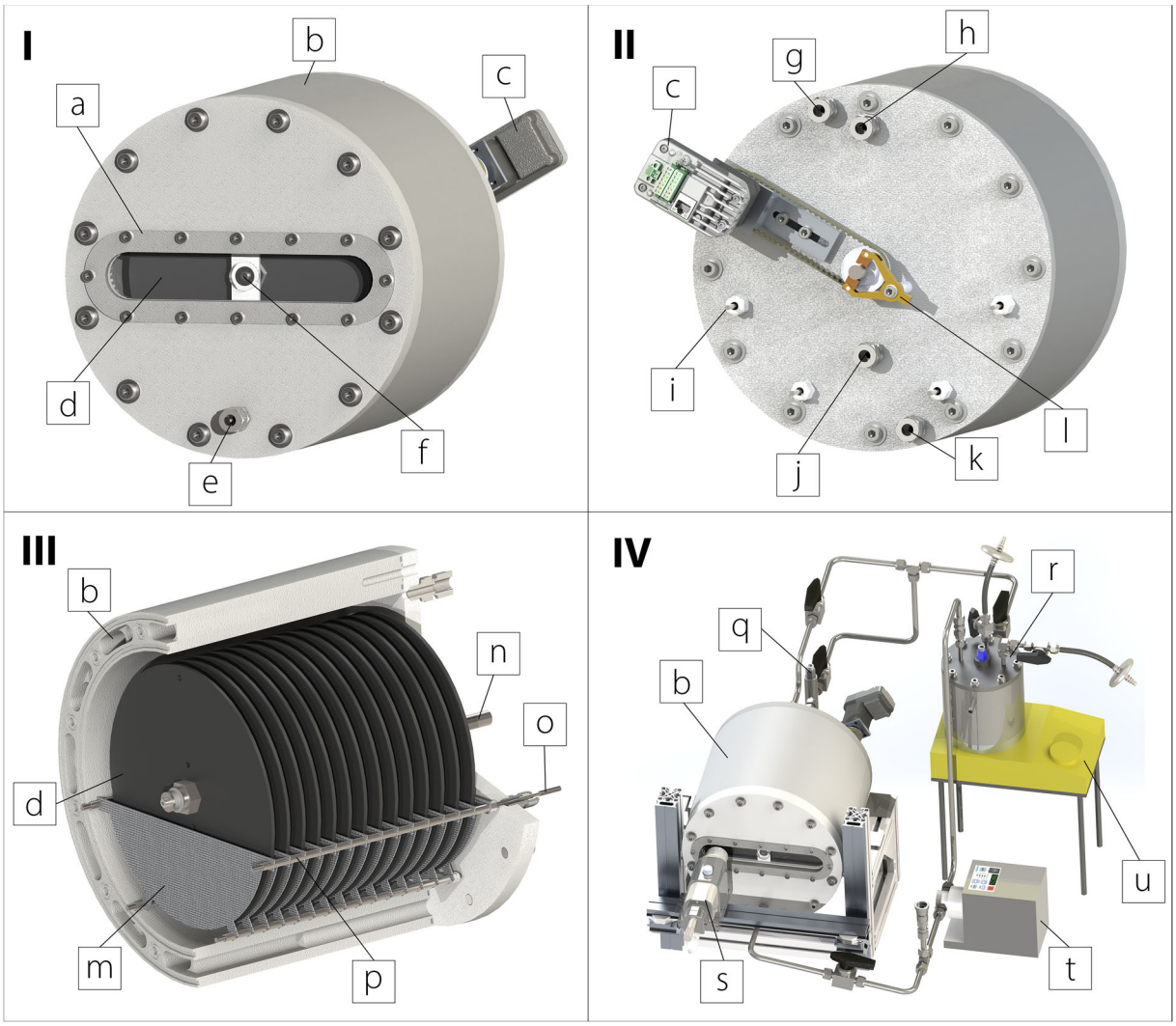


Fig. 1: 3D renderings of the RDBER: (I) Front view of the reaction vessel, (II) rear view of the reaction vessel, (III) cross-section of the reaction vessel, (IV) full system with stainless-steel vessel and piping. (a – inspection window, b – reactor jacket, c – stepper motor , d – working electrode disc, e – inlet to reaction chamber, f – shaft journal bearing, g – outlet of heating jacket, h – gas outlet, i – connector to counter electrode, j – outlet of reaction chamber and connection to reference electrode holder, k – inlet to heating jacket, l – carbon brush holder as connector to rotating working electrodes, m – counter electrodes , n – working electrode shaft , o – counter electrode shaft, p – counter electrode spacers, q – reference electrode, r - double jacketed vessel with integrated pH electrode, s – OCT probe head, t – magnetic gear pump, u – magnetic stirrer).

209 To ensure constant temperatures in the reaction chamber, heating channels were milled into
210 the 31 mm thick polypropylene jacket. These channels were flushed with heating liquid and
211 are shown in the cross-section of the reaction chamber (Fig. 1 III). Inlet (Fig. 1k) and outlet
212 (Fig. 1g) of the heating jacket were placed at the rear flange of the reaction chamber and
213 coupled to a circulation thermostat via clamping ring connections. Simultaneously the growth
214 medium was heated supportively in the optional stainless-steel double jacket vessel during
215 cathodic operation (Fig. 1r). Moreover, the gaseous substrates for electroautotrophic growth
216 were continuously passed through the headspace of the stainless-steel vessel under pressure.
217 The inlet and outlet of the substrate gases are equipped with sterile filters to prevent
218 contamination. By installing a pH electrode (Ceragel CPS71D, Endress + Hauser) in the
219 vessel, the pH value and temperature was logged and the circulation thermostat was regulated.
220 The RDBER was aligned and rigidly fixed on a base frame. Moreover, a holder on which the
221 OCT probe (Fig. 1f) can be fixed was mounted to the base frame.

222

223 **2.2 Strains and preculture conditions**

224 Electroautotrophic experiments were conducted with a population of *K. spormannii* EA-1$^T$
225 previously adapted to cathodic growth (Jung et al., 2020). The preculture for RDBER
226 experiments was grown from freezer stocks in a modified R2A medium (yeast extract 5 g $L^{-1}$,
227 tryptone 1 g $L^{-1}$, casamino acids 0.5 g $L^{-1}$, sodium pyruvate 0.5 g $L^{-1}$, $MgSO_4 \cdot 7\ H_2O$ 0.05 g $L^{-1}$,
228 $K_2HPO_4$ 0.1 g $L^{-1}$, MOPS 10 mM - pH 6) at 60 °C without agitation. The heterotrophically grown
229 pre-culture of *K. spormannii* was washed two times with ES medium (pH 3.5; 10 mM $NH_4Cl$,
230 2.5 mM NaCl, 0.3 mM $KH_2PO_4$, 0.12 mM $MgSO_4$, 0.1 mM $CaCl_2$, 1 ml $L^{-1}$ Wolfe's mineral elixir)
231 before inoculating the autoclaved RDBER setup (Reiner et al., 2018a). Depending on the
232 desired planktonic cell number per working electrode surface ratio the initial optical density
233 ($OD_{600}$) in the RDBER was 0.1 or 0.3 respectively. A counting chamber (Bürker-Türk) was
234 consulted in order to determine the specific cell number per $OD_{600}$ and Volume (an $OD_{600}$ of 1
235 corresponded to 3.16±0.25 *K. spormannii* cells per ml).

236 A mixed culture of the model organisms *Shewanella oneidensis* MR-1 and *Geobacter*
237 *sulfurreducens* PCA was employed as biocatalyst during anodic operation of the RDBER.
238 *S. oneidensis* was precultured aerobically in LB-Medium (Lennox), while the cultivation of the
239 *G. sulfurreducens* preculture was conducted under anoxic conditions in BES-Medium
240 [0.42 g $L^{-1}$ $KH_2PO_4$, 0.22 g $L^{-1}$ $K_2HPO_4$, 0.2 g $L^{-1}$ $NH_4Cl$, 0.38 g $L^{-1}$ KCl, 0.36 g $L^{-1}$ NaCl,
241 0.21 g $L^{-1}$ $MgCl_2$, 11.92 g $L^{-1}$ HEPES – after autoclaving the medium was complemented with
242 1 ml $L^{-1}$ 0.4 mM $CaCl_2$ solution, 10 ml $L^{-1}$ NB trace mineral solution, 1.0 ml selenite–tungstate
243 solution (13 mM NaOH, 17 µM $Na_2SeO_3$, and 12 µM $Na_2WO_4$), 10 ml vitamin solution (German
244 Type Culture Collection, DSMZ, media 141) and then sparged in rubber sealed bottles with
245 $N_2/CO_2$ (80:20 vol%) for 30 minutes]. For preculturing, the BES-medium was complemented
246 with 20 mM sodium acetate as electron donor and disodium fumarate (40 mM) as electron
247 acceptor. The final pH was set to 7.4. Before inoculating the reactor with a mixture of
248 *G. sulfurreducens* and *S. oneidensis* in a 9 to 1 ratio to an initial $OD_{600}$ of 0.1, the cells were
249 washed two times in BES-Medium.

250

251 **2.3 Cultivation of cathodic *K. spormannii* biofilms**

252 After pumping the previously inoculated ES-Medium into the sterile RDBER, the medium
253 temperature was adjusted to 60 °C. The headspace of the mixing vessel was pressurized to
254 0.5 bar and continuously flushed with a mixture of 99.5% $CO_2$ (v/v) and 0.5% $O_2$ (v/v) while the
255 liquid phase was continuously stirred at 300 rpm. The additional stirring of the medium in the
256 mixing vessel by means of a magnetic stirrer (Fig. 1u) ensured improved mass transfer of the
257 gases and increased the heat transfer of the heated jacket into the medium. The cultivation
258 medium enriched with the gaseous substrates was pumped through the RDBER at a constant
259 volumetric flow rate of 500 ml $min^{-1}$. In order to achieve different planktonic cell number per
260 working electrode surface ratios, either only one or all electrodes were mounted (714 $cm^2$ vs.
261 1 $m^2$ working electrode surface). The rotational speed of the working electrodes amounted to
262 one revolution per minute. A constant current density of 1 µA $cm^{-2}$ was applied for 24 h
263 immediately after inoculation by means of a potentiostat (Interface 5000P, Gamry Instruments,

264 Warmister, USA). After this initial polarization phase, the current density was set to 3 μA $cm^{-2}$
265 by the end of the experiment. The experiments were stopped upon detection of no further
266 biofilm increase.
267

268 **2.4 Anodic operation as Microbial Electrolysis Cell**

269 10 L of inoculated BES-medium containing 20 mM sodium acetate and 20 mM sodium lactate
270 as carbon source was pumped in the previously autoclaved RDBER. Chronoamperometric
271 batch experiments were performed at 30 °C and a constant working electrode potential of 0 mV
272 vs. SHE (standard hydrogen electrode) was set. For anodic operation the stainless-steel
273 mixing vessel was omitted while the pipeline was shorted with a pH-electrode holder. Evolving
274 reaction gases (e.g. Hydrogen and $CO_2$) were collected at the upper outlet (Fig. 1h) and led
275 through a MilliGascounter (Ritter, Germany) into a gas sampling bag. Analysis of collected
276 gases was conducted by means of a Micro GC (490 Micro GC, Agilent Technologies,
277 Germany) using two different carrier gases (argon and helium) and two stationary phases (CP-
278 Molsieve 5 Å Plot and PoraPLOT U J&W GC columns, Agilent Technologies, Germany).
279 Moreover, liquid samples were taken twice a day in order to quantify the concentration of
280 organic acids by means of a Metrohm 881 Compact Pro Ion Exchange Chromatograph with a
281 Metrosep Organic Acids 250/7.8 column (Metrohm, Switzerland).

282

283 **2.5 OCT imaging and digital image processing**

284 A GANYMEDE II spectral domain OCT system (Thorlabs GmbH, Dachau, Germany) equipped
285 with a LSM04 objective lens was employed for 3D biofilm visualization (Thorlabs GmbH,
286 Dachau, Germany). Prior to each OCT acquisition, the stepper motor was consistently halted
287 in the same pre-assigned position. Together with the fixed position of the OCT probe holder,
288 this allowed reproducible visualization of a selected radial cathode section. OCT 3D data sets
289 (C-scans) were acquired regularly over the visualizable radial area (see Fig. 2). Each spot was
290 scanned with a size of 10.0 mm × 6.0 mm × 2.0 mm (L × W × H) and pixel resolutions of

8 µm $px^{-1}$ (lateral, xy-plane) and 2.06 µm $px^{-1}$ (axial, z-direction). Adjacent OCT data sets were then stitched to depict the whole radius of the cathode. The generated OCT datasets were then analyzed, merged, and finally assembled into a height profile (6 mm × 70 mm; H × W). The visualized rectangular area was then trimmed into an isosceles trapezoid for final evaluation. The trapezoid represents a circular sector of the round disk, which abuts the outer radius of the substrate and was shortened to 70 mm by cutting off the tip. 110 of these trapezoids could thus be approximately combined to form a circular ring with an outer diameter of 21 mm and an inner diameter of 70 mm. Finally, the mean biovolume $\overline{BV}$, the mean accumulation rate $\overline{BV}^*$, and the mean coverage $\overline{SC}$ over the radius were determined from the cropped trapezoid (detailed view Figure 2). In addition, the trapezoid was divided into 7 further 10 mm long sub-trapezoids to obtain detailed information about the spatial distribution of biovolume ($BV$) along the radius of the circular blank. ImageJ [23], operated with in-house made macros [24], was used to calculate topographic representations of the bulk-biofilm interface (height maps) and the structural parameters used for biofilm characterization.

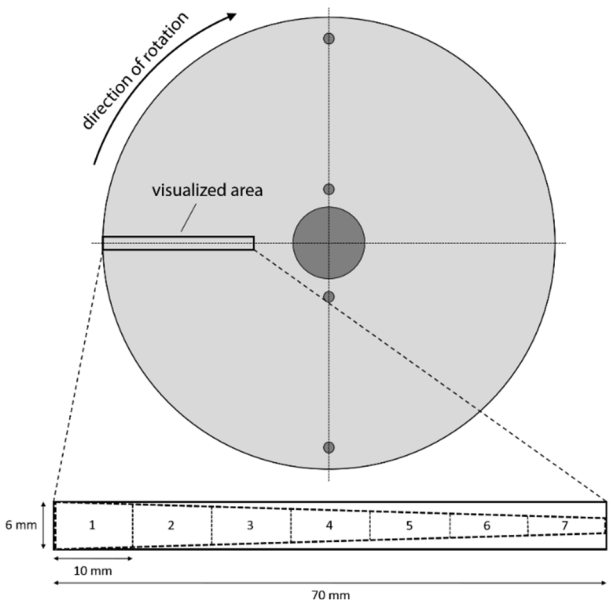


Fig. 2: Representation of the visualized area and the analyzed trapezoidal sections of the generated OCT data sets.

### 2.6 Parameters for biofilm characterization

The calculation of the biofilm structure parameters - biovolume $BV$ (µm$^3$ µm$^{-2}$), mean biovolume $\overline{BV}$ (µm$^3$ µm$^{-2}$), mean biofilm accumulation rate $\overline{BV}^*$ (µm$^3$ µm$^{-2}$ d$^{-1}$) and mean substratum coverage $\overline{SC}$ (-) was based on height maps according to Wagner and Horn(Wagner and Horn, 2017).

Biovolume $BV$ is defined as the measured biofilm volume $V_{BF}$ (µm$^3$) per specific area of a single small trapezoid $A_{ST}$ (µm$^2$)

$$BV = \frac{V_{BF}}{A_{ST}}$$

whereas $\overline{BV}$ is being defined as

$$\overline{BV} = \frac{\sum V_{BFn}}{\sum A_{STn}}$$

Where $n$ indexes the individual small trapezoids.

Mean biofilm accumulation rate $\overline{BV}^*$ corresponds to $\overline{BV}$ derived by time:

$$\overline{BV}^* = \frac{\partial \overline{BV}}{\partial t}$$

Finally, mean substratum coverage $\overline{SC}$ is described as

$$\overline{SC} = \frac{\sum A_{STn} - A_{uc}}{\sum A_{STn}}$$

342 with the area of uncovered substratum $A_{uc}$ (biofilm thickness = 0 µm).

343

344 ## 3. Results and discussion

345 ### 3.1 Cultivation of cathodic *K. spormannii* biofilms

346 In order to prove the functionality of the newly developed reactor concept, two different pure
347 culture cultivations of electroactive microorganisms were performed in the RDBER. Moreover,
348 initial cultivation experiments performed with *K. spormannii* were designed to answer the
349 question of whether an RBC-like reactor could even be a potential technological platform for
350 upscaling a biofilm-based, aerobic MES process that was previously demonstrated in small-
351 scale, custom-made flow cells (Hackbarth et al., 2020; Jung et al., 2020). Thus, as many
352 process parameters as possible were transferred from the established flow cell cultivation to
353 the cultivation of *K. spormannii* in the RDBER (see Table 1). Hence, for preliminary cultivation
354 experiments the previously autoclaved RDBER was filled with sterile ES-Medium (pH 3.5),
355 omitting any organic carbon source and inoculated with *K. spormannii* to an initial $OD_{600}$ of 0.1.
356 In order to increase their solubility, the system was then pressurized to 0.5 bars with the
357 substrate gases $CO_2$ and $O_2$ and the mediums temperature was set to 60 °C. The rotational
358 speed of the cathodes amounted to 1 rpm. After several days of reactor operation, OCT
359 analysis of the cathode revealed isolated tower-like structures formed on the cathode.
360 However, their quantity and height decreased sharply again in the course of a few days (see
361 Supplementary Fig. 1). Moreover, the surface coverage of the substratum never exceeded
362 20% even after one month of cultivation. In summary, no continuous biofilm could be detected
363 on the cathodes by OCT during the preliminary cultivations. When examined more closely,
364 there were two particular process parameters that deviated from the flow cell experiments due
365 to the entirely divergent reactor concept of the RDBER: Firstly, the initial cell number per
366 cathode area, and secondly, the hydraulic retention time in the reaction chamber (0.5 min in
367 the flow-cells compared to 18.4 min in the RDBER). However, since in an RBC-like reactor the
368 flow velocity over the substratum depends on the angular velocity of the substrate rather than

369 the hydraulic residence time (HRT), we assumed that HRT was not likely to be the key process
370 parameter that hindered biofilm growth during the preliminary cultivation experiments. In
371 particular, because care was taken to ensure that the angular velocity of the circular blank at
372 the outermost radius should not exceed the optimum flow velocity for cultivation of *K.*
373 *spormannii* in the flow cell system. Using the circumference of the circular blanks, it was
374 calculated that a velocity of 11 mm $s^{-1}$ is achieved at the outermost radius at a rotational speed
375 of 1 U $min^{-1}$, which is within the range of the flow velocity over the cathode in the flow cell
376 system based on the previously conducted CFD simulation (Hackbarth et al., 2020). Hence,
377 we hypothesized, that the 44 times lower initial cell number per cathode surface ratio
378 ($3.4 * 10^9$ $cm^{-2}$ in the flow-cells vs. $7.6 * 10^7$ $cm^{-2}$ for the preliminary RDBER experiments) might
379 be the limiting factor for consistent biofilm growth.

380

381

382

383

384

385

386

387

388

389

390

391

392 Table 1: Listing of important process parameters comparing the RDBER cultivations of *K. spormannii*
393 performed in this study and flow cell cultivations performed in another study. LSV – Linear sweep
394 voltammetry, CA – Chronoamperometry.

| **Process parameter** | **Flow-cell cultivation [18]** | **Preliminary cultivation (this study)** | **Optimized cultivation (this study)** |
|---|---|---|---|
| **Medium** | ES-medium | Es-medium | Es-medium |
| **pH** | 3.5 | 3.5 | 3.5 |
| **Gas mixture** | $CO_2/O_2$ (99.5:0.5) | $CO_2/O_2$ (99.5:0.5) | $CO_2/O_2$ (99.5:0.5) |
| **Pressure** | 1.5 bar | 0.5 bar | 0.5 bar |
| **Temperature** | 60 °C | 60 °C | 60 °C |
| **Circulation pump speed** | 100 ml $min^{-1}$ | 500 ml $min^{-1}$ | 500 ml $min^{-1}$ |
| **Volume $_{reaction\ chamber}$** | 50 ml | 8500 ml | 9850 ml |
| **Hydraulic retention time** | 0.5 min | 17 min | 19.7 min |
| **Flow velocity / angular velocity over / of substratum at r = 210 mm** | up to 21 mm $s^{-1}$ | up to 11 mm $s^{-1}$ | up to 11 mm $s^{-1}$ |
| **Electroanalytics** | potentiostatic LSV (first 24 h), then CA (-500 mV vs. SHE) | potentiostatic LSV (first 24 h), then CA (-500 mV vs. SHE) | galvanostatic 1 µA $cm^{-2}$ (first 24 h), then 3 µA $cm^{-2}$ |
| **Volume $_{system}$ (incl. pipes, etc.)** | 850 ml | 9500 ml | 10850 ml |
| **Initial $OD_{600}$** | 0.1 | 0.1 | 0.3 |
| **Working Electrode Surface** | 20 $cm^2$ | 10000 $cm^2$ | 700 $cm^2$ |
| **Initial cell number per working electrode ratio** | 1.34 * $10^9$ $cm^{-2}$ | 3.0 * $10^7$ $cm^{-2}$ | 1.47 * $10^9$ $cm^{-2}$ |

395

396

397

398

399

400 Previously it was shown that at the initially uncovered cathode a part of the dissolved oxygen
401 might be abiotically reduced into reactive oxygen species (ROS) (Hackbarth et al., 2020; Jung
402 et al., 2020). As the initial cell number decreases, the cumulative ROS-detoxification capacity
403 of the cells also decreases, possibly preventing a sufficient initial cathode coverage that serves
404 as an insulator to minimize abiotic ROS formation. Therefore, we adjusted the cell number to
405 cathode surface ratio for the subsequent experiments. Besides increasing the initial $OD_{600}$ from
406 0.1 to 0.3, we also reduced the working electrode area to 700 $cm^2$, in order to avoid the need
407 of a tremendous amount of preculture, which would not have been cultivatable in our laboratory
408 infrastructure yet. Furthermore, the current density of the system was limited by galvanometry
409 to 1 µA $cm^{-2}$ for 24 h (and then to 3 µA $cm^{-2}$ for the rest of the experiment) to minimize initial
410 ROS-formation. Operation of the RDBER under adapted process conditions now resulted in
411 the formation of nearly continuous *K. spormannii* biofilms covering more than 90% of the
412 cathode. Figure 3 shows a timeseries of height maps derived from OCT datasets covering a
413 radial excerpt of the working electrode.

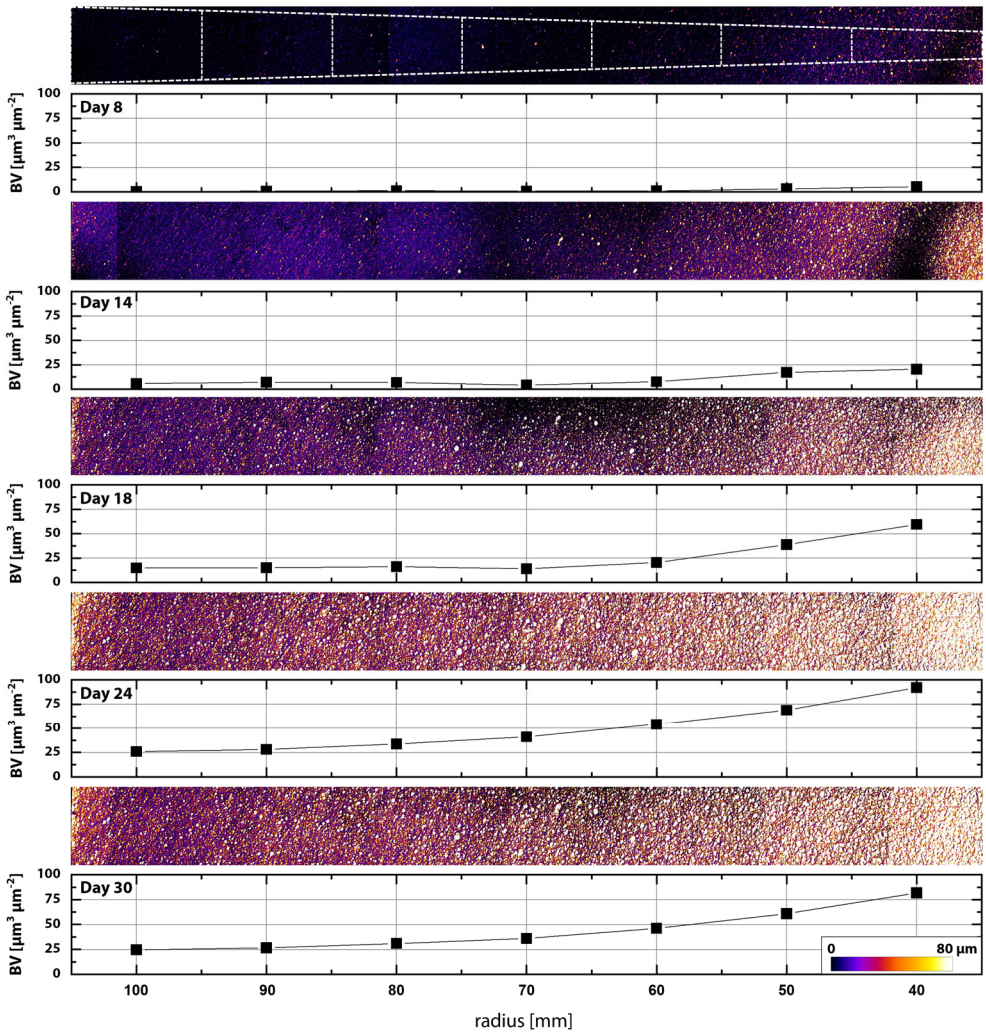


Fig. 3: Time series of selected OCT-derived height maps of the optimized cultivation of *K. spormannii* in the 10 L-RDBER. The same radial section has been visualized on the working electrode in each case in order to show the spatial distribution of the biofilm along the rotating working electrode. Colors are coded from black (0 mm) to white (80 µm). The calculated biovolumes ($BV$) of the subtrapezoids are shown below the height profiles.

The first visible biofilm structures formed after a lag phase of 8 days near the shaft, i.e. at regions with comparatively low shear stress. A spatially resolved calculation of the local biovolume clearly shows that $BV$ decreases with larger radius towards the edge of the circular blank. So, with an increased angular velocity of the substratum and therefore a higher flow velocity over the biofilm, the biovolume of the *K. spormannii* biofilm is decreasing. After 24 days $BV$ reached the maximum values measured in the course of the experiment in all segments. The maximum $BV$ in the outer region of the cathode averaged 25 $\mu m^3\ \mu m^{-2}$, only about a quarter of the max $BV$ of approximately 100 $\mu m^3\ \mu m^{-2}$ observed in the inner visualized region. It should also be mentioned that in an abiotic control experiment, no growth-like precipitation was detected on the cathodes after 24 days. The extent to which the biovolume can be used to draw conclusions about the productivity (i.e., $CO_2$-fixation rate) of the *K. spormannii* biofilm is not conclusive from this data. Nevertheless, it is known that compressed and denser biofilms generally exhibit higher turnover rates, since more catalytically active biomass is present per biovolume. At the same time, denser biofilm structures might hamper the diffusion of substrates and products within the biofilm (de Beer et al., 1994; Horn and Morgenroth, 2006), whereas the heterogeneity of the biofilm structure will also influence diffusion reaction (van den Berg et al., 2020). Certainly, the increased shear force at increased angular velocity affects the biofilm height to some extent as well. This effect may also be exploited in a future biotechnological process. Thus, a fluctuating and short-term increase of the rotational speed could serve for an optimal harvesting of the biomass from the substratum. In this way, the planktonic biomass could be partially and discontinuously extracted from the reactor, creating a self-sustaining system, since some of the detached cells can recolonize uncovered areas of the substratum. In order to compare the results of the RDBER system with those of the previously published flow cell experiments, calculated $\overline{BV}$ values were fitted by a logistic growth function:

$$\overline{BV} = 40.718 + (3.055 - 40.718) / (1 + (t / 17.765)^{11.14}) \quad (R^2 = 0.98)$$

The course of the plotted values of $\overline{BV}$ shows a significantly longer lag phase compared to the flow cell experiments. The highest biofilm accumulation rate of 6 $\mu m^3\ \mu m^{-2}\ d^{-1}$ was reached between days 17 and 18 and was 45% lower compared to the flow cell experiments (see figure

452 6 in [12]). Moreover, the maximal achieved mean biovolume in the RDBER system was
453 42 $\mu m^3$ $\mu m^{-2}$, which accounted to around 25% of the max. mean biovolume in the flow-cells.
454 The highest coverage of 87% was reached on day 24, with $\overline{SC}$ not describing a steeply
455 increasing degressive course like in the flow-cell experiments, but a linear course until the
456 biofilm finally detached. The biofilm in the RDBER system thus showed a generally weaker
457 and slower growth per area of cathode surface. Notwithstanding, to our knowledge, this data
458 shows the first successful cultivation of an aerobic, electroautotrophic organism in a BES at
459 this scale (700 $cm^{-2}$ working electrode). One of the reasons for the comparatively slow growth
460 of *K. spormannii* in the RDBER was probably the moderate, limited current density (3 µA $cm^{-2}$)
461 - especially in contrast to the measured currents of the flow cell experiments (between 13 and
462 20 µA $cm^{-2}$ at a constant working electrode potential of -500 mV vs. SHE). Although excessive
463 ROS production does not occur if the current density is too low, the biocatalyst may not have
464 enough electrons available for rapid and, above all, complete coverage of the substrate. Thus,
465 in future experiments, the maximum current density should be limited to that extent only during
466 the initial start-up phase and should also be increased as the surface coverage increases.

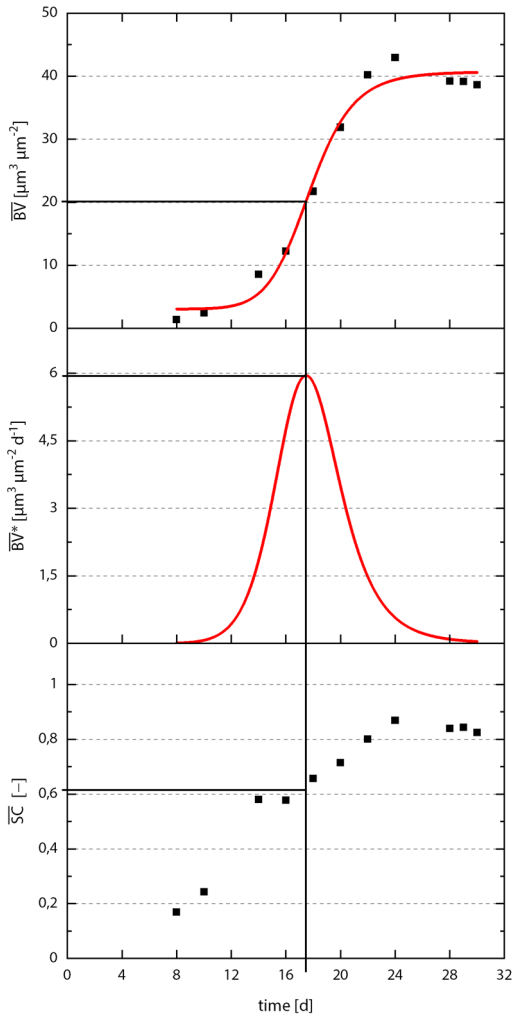


467

468 Fig. 4: Plot of calculated biofilm parameters of the optimized cathodic operation of the RDBER
469 over time [mean biovolume ($\overline{BV}$), mean biofilm accumulation rate ($\overline{BV}^*$), and mean substrate
470 coverage ($\overline{SC}$)].

471

472

473

474

475

476

477 In addition to the limitation of the electron donor, reduced substrate availability due to lower
478 solubility of the gaseous substrates at reduced pressure in the RDBER (0.5 bar) compared to
479 the flow cells (1.5 bar) has to be assumed. Indeed, in their computational model of a microbial
480 electrosynthesis process, Cabau-Peinado et al. demonstrated that $CO_2$ limitations can occur
481 and thus may play a role in low turnover rates of a MES system (Cabau-Peinado et al., 2021).
482 According to the manufacturer, the shaft seal of the titanium shaft in the rear flange is currently
483 the only tender spot that limits the maximum pressure in the system to 0.5 bar. Both the reactor
484 periphery and the entire reactor jacket can be pressurized to at least 1.5 bar. Therefore, future
485 reactor generations should incorporate a shaft seal in the rear bearing that is designed for
486 higher pressure ranges in order to assess the impact of the pressure on the biofilm
487 development in the RDBER.

488

489 **3.2 Anodic operation as Microbial Electrolysis Cell**

490 Following the successful cultivation of an electroautotrophic species in the RDBER, we used
491 the reactor to cultivate a defined coculture of *Shewanella oneidensis* and *Geobacter*
492 *sulfurreducens*. Both organisms are well-studied electroactive model organisms for
493 extracellular electron transfer of respiratory electrons to insoluble electron acceptors such as
494 an anode of a BES. The anodic operation of the RDBER as a microbial electrolysis cell (MEC)
495 was intended not only to prove the basic functionality of the system, but also to emphasize the
496 flexibility regarding the possible applications of the RDBER. In a MEC, electroactive organisms
497 oxidize organic matter into $CO_2$ and protons, whereby the released electrons are transferred
498 from the organisms to the anode, which serves as a terminal respiratory electron acceptor.
499 From the anode, the electrons are transferred to the cathode by means of a current source.
500 Subsequently, protons are then reduced to hydrogen at the cathode. The experiments were
501 performed as batch experiments with a full set of the 14 working electrodes (here anodes) with
502 a total surface area of 1 $m^2$ at a rotational speed of 1 rpm. Acetate and lactate served as carbon
503 source with an initial concentration of 20 mM each. The current density at a constant working

electrode potential of 0 mV vs. SHE was recorded over the experimental course of roughly 9 days (see Fig 5). After an initial polarization phase of a few hours, characterized by negative current densities most likely due to the depletion of residual oxygen in the system, the current steadily increased until it peaked at 130 μA $cm^{-2}$ after about 4 days. Subsequently, the current density drops again to slowly decrease to about 90 μA $cm^{-2}$ after 9 days. Almost uniform in shape runs the graph of the gas evolution rate recorded by means of a MilliGascounter from the gas outlet of the RDBER. The hydrogen fraction in the outflowing gas was examined regularly using a MicroGC and remained almost constant over the entire experimental period (88.1 ± 1.2%). Daily liquid sampling of the reactor's broth was conducted to determine the concentration of the organic acids via ion chromatography.

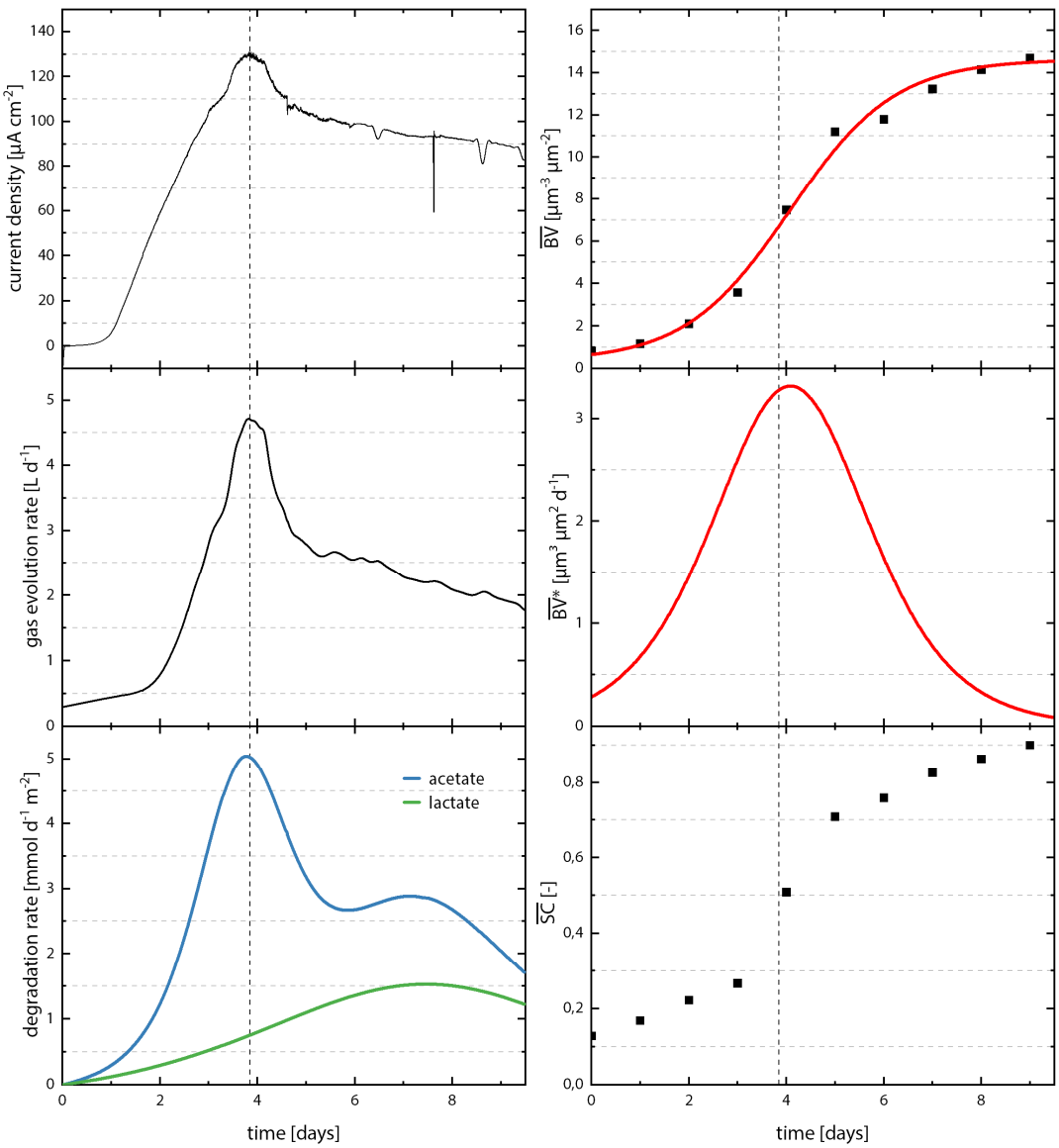


Fig. 5: Correlation of current density, gas evolution rate and substrate specific degradation rate with calculated biofilm parameters obtained during anodic operation of the RDBER. A coculture of *Shewanella oneidensis* and *Geobacter sulfurreducens* was cultivated at a working electrode potential of 0 mV vs. SHE in a MEC-like operation. For a clearer representation, the graphs of current density and gas evolution rate were smoothed with an FFT filter. Raw data of organic acid concentrations, as well as the applied fits (displayed in color), are provided in the Supplementary Material.

525 The course of the concentration values over time was fitted and derived after time to obtain
526 the specific degradation rates for acetate and lactate, respectively (please refer to the
527 supplementary material for original data and fit). In this context, it was important to consider
528 that *Shewanella* degrades one molecule of lactate into one molecule of acetate and $CO_2$ or
529 formate. Since the acetate concentration did not increase during the experiment, it was
530 therefore assumed that the acetate produced by *Shewanella* was directly metabolized by
531 *Geobacter*. This was taken into account when calculating the specific acetate degradation rate.
532 Since both the peak in current data, and in the gas production rate, correlate with the peak in
533 acetate degradation rate on day 4, these data clearly demonstrate that *Geobacter* is
534 accounting for most of the current production, as *Shewanella* is not capable of metabolizing
535 acetate. The maximum degradation rate for acetate was 5 mmol $d^{-1}$ $m^{-2}$ cathode surface and
536 1.5 mmol $d^{-1}$ $m^{-2}$ for lactate, respectively. Regular OCT scans of a radial anode section
537 provided the basis for calculating $\overline{BV}$ and $\overline{SC}$. Figure 5 shows the mean biofilm accumulation
538 rate ($\overline{BV}^*$) derived from a logarithmic fit through the calculated $\overline{BV}$ values:

539 $\overline{BV} = 0.343 + (14.646 - 0.343) / (1 + 10^{((4.083 - t) * (0.404))})$ ($R^2 = 0.99$)

540 The highest biofilm accumulation rate of almost 3 $\mu m^3$ $\mu m^{-2}$ $d^{-1}$ is likewise reached after about
541 4 days. Again, based on the correlations with the degradation rate, conclusions can be drawn
542 that *Geobacter* cells appear to be the predominant species in the biofilm. This is also consistent
543 with the literature findings that attribute rather modest biofilm capabilities to *Shewanella*
544 compared to *Geobacter* (Engel et al., 2019). After 9 days the anodic biofilm covered around
545 90% of the observed working electrode surface. Interestingly, the mean surface coverage does
546 not increase linearly as in the cathodic cultivation experiments of *K. spormannii*, but rather
547 logarithmically. Hence, it can be concluded that the growth pattern seen in the cathodic
548 experiments is not so much an intrinsic phenomenon of the RDBER, but probably due to the
549 abiotic formation of ROS on uncovered cathodes described above. Comparing the
550 performance of the RDBER with other single-chamber upscaling attempts of MECs, it is
551 apparent on the one hand that there is still room for improvement in terms of current densities,
552 but on the other hand the excellent surface to reactor volume ratio (100 $m^2$ $m^{-3}$) of the RDBER

553 is worth emphasizing (Enzmann et al., 2018). For example, Brown et al. measured current
554 densities up to 720 µA $cm^{-2}$, but at a surface to volume ratio of 15 $m^2$ $m^{-3}$ (0.58 $m^2$ anode area
555 and 30 L reactor volume) (Brown et al., 2014). In another study, the measured maximum
556 current densities were in similar ranges around 700 µA, but again with a surface to volume
557 ratio five times lower than in the RDBER (Cusick et al., 2011). However, it should be noted that
558 the experiments conducted here were only short-term batch experiments to validate the
559 functionality of the system. The above studies were conducted in a continuous operating mode
560 for a significantly longer period of time, up to several months, allowing a more productive
561 biofilm to grow on the working electrode over the longer cultivation period. In addition, the ion
562 chromatographic data also indicate that the biofilm may have already reached a degree of
563 substrate limitation (original data in supplementary material). Furthermore, the optimal
564 rotational speed of the working electrodes must be identified for each future application of the
565 RDBER and thus for each specific microbial community specifically.

566

567 **4. Conclusions**

568 In conclusion, the study aimed on the design of a novel, scalable electrochemical reactor
569 concept that meets the requirements of biotechnological pure culture cultivations. During the
570 construction of the single-chamber system, emphasis was laid on a long operating lifetime and
571 low-maintenance operation. The successful cultivation of different electroactive model
572 organisms, both in anodic and cathodic operation, prove on the one hand the basic functionality
573 of the system. On the other hand, we were able to demonstrate that an increase in the working
574 electrode area is not only possible by numbering up individual small reactor systems, as is
575 often the case for METs. If microbial electrochemical technologies are to become truly
576 competitive, a greater range of creative reactor designs that can be scaled up without
577 excessive numbering-up is necessary. A further scale-up of the RDBER is conceivable as well:
578 While the diameter of the electrode discs is limited mainly by the angular velocity at the outer
579 edge, the shaft can be extended (and equipped with more electrodes) until it is unable to

statically support its own weight. Moreover, based on this work, we were able to show that an RBC-like reactor is, in principle, a feasible way to upscale the previously flow cell-based cultivation of *K. spormannii* for bioplastic production from electricity and $CO_2$. Since the pumping power required for successful cultivation of *K. spormannii* in an upscaled flow cell process would presumably render the overall process quickly uneconomical, an RBC-like reactor might be an interesting option to generate HRT independent crossflow velocities across the working electrode. Furthermore, the cultivation experiments of *K. spormannii* in the RDBER highlighted the crucial role of the start-up phase in aerobic MES processes. The impact of reactive oxygen species should not be underestimated in the development of future MES processes. Therefore, for the necessary development of targeted strategies, it is important to better understand the formation of reactive oxygen species at cathodes under physiological conditions, as well as the different detoxification mechanisms of electroautotrophic microorganisms.

## 5. Funding

This work was supported by a grant of the Federal Ministry of Education and Research (BMBF) as part of the BioElectroPlast project, no. 033RC006.

## 6. Declaration of Competing Interest

The authors declare that they have no known competing financial interests or personal relationships that could have appeared to influence the work reported in this paper.

## 7. Acknowledgements

Special thanks go to Prof. Harald Horn for the initial idea behind the reactor concept, to Axel Heidt as the person responsible for the IC measurements and to Erwin Wachter, Joachim Lang

606 and Alfred Herbst from the metal workshop of the EBI for their work and support during the
607 construction of the reactor.

608

## 609 8. CRediT authorship contribution statement

610 **Max Hackbarth:** Investigation, Conceptualization, Methodology, Visualization. **Johannes**
611 **Gescher:** Conceptualization, Writing - Review & Editing, Funding acquisition. **Harald Horn:**
612 Conceptualization, Writing - Review & Editing, Funding acquisition. **Johannes Eberhard**
613 **Reiner:** Investigation, Conceptualization, Methodology, Visualization, Writing - Original Draft
614 & Editing.

615

## 616 9. References

617 Barham, P.J., Keller, A., Otun, E.L., Holmes, P.A., 1984. Crystallization and morphology of a bacterial
618 thermoplastic: poly-3-hydroxybutyrate. J Mater Sci 19, 2781–2794.
619 https://doi.org/10.1007/BF01026954

620 Brown, R.K., Harnisch, F., Wirth, S., Wahlandt, H., Dockhorn, T., Dichtl, N., Schröder, U., 2014.
621 Evaluating the effects of scaling up on the performance of bioelectrochemical systems using a
622 technical scale microbial electrolysis cell. Bioresour Technol 163, 206–213.
623 https://doi.org/10.1016/J.BIORTECH.2014.04.044

624 Cabau-Peinado, O., Straathof, A.J.J., Jourdin, L., 2021. A General Model for Biofilm-Driven Microbial
625 Electrosynthesis of Carboxylates From $CO_2$. Front Microbiol 12, 1405.
626 https://doi.org/10.3389/FMICB.2021.669218/BIBTEX

627 Cheng, K.Y., Ho, G., Cord-Ruwisch, R., 2012. Energy-efficient treatment of organic wastewater
628 streams using a rotatable bioelectrochemical contactor (RBEC). Bioresour Technol 126, 431–
629 436. https://doi.org/10.1016/J.BIORTECH.2011.12.011

630 Cheng, K.Y., Ho, G., Cord-Ruwisch, R., 2011. Novel methanogenic rotatable bioelectrochemical
631 system operated with polarity inversion. Environ Sci Technol 45, 796–802.
632 https://doi.org/10.1021/ES102482J/SUPPL_FILE/ES102482J_SI_001.PDF

633 Christodoulou, X., Velasquez-Orta, S.B., 2016. Microbial electrosynthesis and anaerobic
634 fermentation: An economic evaluation for acetic acid production from $CO_2$ and CO. Environ Sci
635 Technol acs.est.6b02101. https://doi.org/10.1021/acs.est.6b02101

636 Cortez, S., Teixeira, P., Oliveira, R., Mota, M., 2008. Rotating biological contactors: A review on main
637 factors affecting performance. Rev Environ Sci Biotechnol 7, 155–172.
638 https://doi.org/10.1007/S11157-008-9127-X/TABLES/4

639 Cusick, R.D., Bryan, B., Parker, D.S., Merrill, M.D., Mehanna, M., Kiely, P.D., Liu, G., Logan, B.E., 2011.
640 Performance of a pilot-scale continuous flow microbial electrolysis cell fed winery wastewater.
641 Appl Microbiol Biotechnol 89, 2053–2063. https://doi.org/10.1007/S00253-011-3130-9

642 de Beer, D., Stoodley, P., Roe, F., Lewandowski, Z., 1994. Effects of biofilm structures on oxygen
643 distribution and mass transport. Biotechnol Bioeng 43, 1131–1138.
644 https://doi.org/10.1002/BIT.260431118

645 Engel, C., Schattenberg, F., Dohnt, K., Schröder, U., Müller, S., Krull, R., 2019. Long-Term Behavior of
646 Defined Mixed Cultures of *Geobacter sulfurreducens* and *Shewanella oneidensis* in
647 Bioelectrochemical Systems. Front Bioeng Biotechnol 7.
648 https://doi.org/10.3389/FBIOE.2019.00060

649 Enzmann, F., Mayer, F., Stöckl, M., Mangold, K.M., Hommel, R., Holtmann, D., 2019. Transferring
650 bioelectrochemical processes from H-cells to a scalable bubble column reactor. Chem Eng Sci
651 193, 133–143. https://doi.org/10.1016/J.CES.2018.08.056

652 Enzmann, F., Stöckl, M., Zeng, A.-P., Holtmann, D., 2018. Same but different-Scale up and numbering
653 up in electrobiotechnology and photobiotechnology. https://doi.org/10.1002/elsc.201800160

654 Gildemyn, S., Verbeeck, K., Jansen, R., Rabaey, K., 2017. The type of ion selective membrane
655 determines stability and production levels of microbial electrosynthesis. Bioresour Technol 224,
656 358–364. https://doi.org/10.1016/J.BIORTECH.2016.11.088

657 Guo, K., Prévoteau, A., Patil, S.A., Rabaey, K., 2015. Engineering electrodes for microbial
658 electrocatalysis. Curr Opin Biotechnol 33, 149–156.
659 https://doi.org/10.1016/J.COPBIO.2015.02.014

660 Guo, K., Prévoteau, A., Rabaey, K., 2017. A novel tubular microbial electrolysis cell for high rate
661 hydrogen production. J Power Sources 356, 484–490.
662 https://doi.org/10.1016/J.JPOWSOUR.2017.03.029

663 Hackbarth, M., Jung, T., Reiner, J.E., Gescher, J., Horn, H., Hille-Reichel, A., Wagner, M., 2020.
664 Monitoring and quantification of bioelectrochemical *Kyrpidia spormannii* biofilm development
665 in a novel flow cell setup. Chemical Engineering Journal 390, 124604.
666 https://doi.org/10.1016/J.CEJ.2020.124604

667 Hassard, F., Biddle, J., Cartmell, E., Jefferson, B., Tyrrel, S., Stephenson, T., 2015. Rotating biological
668 contactors for wastewater treatment – A review. Process Safety and Environmental Protection
669 94, 285–306. https://doi.org/10.1016/J.PSEP.2014.07.003

670 Horn, H., Morgenroth, E., 2006. Transport of oxygen, sodium chloride, and sodium nitrate in biofilms.
671 Chem Eng Sci 61, 1347–1356. https://doi.org/10.1016/J.CES.2005.08.027

672 Jourdin, L., Burdyny, T., 2021. Microbial Electrosynthesis: Where Do We Go from Here? Trends
673 Biotechnol 39, 359–369. https://doi.org/10.1016/J.TIBTECH.2020.10.014

674 Jourdin, L., Sousa, J., Stralen, N. van, Strik, D.P.B.T.B., 2020. Techno-economic assessment of
675 microbial electrosynthesis from $CO_2$ and/or organics: An interdisciplinary roadmap towards
676 future research and application. Appl Energy 279, 115775.
677 https://doi.org/10.1016/J.APENERGY.2020.115775

678 Jung, T., Hackbarth, M., Horn, H., Gescher, J., 2020. Improving the Cathodic Biofilm Growth
679 Capabilities of *Kyrpidia spormannii* EA-1 by Undirected Mutagenesis. Microorganisms 2021, Vol.
680 9, Page 77 9, 77. https://doi.org/10.3390/MICROORGANISMS9010077

681 Kerzenmacher, S., 2017. Engineering of Microbial Electrodes. Springer, Berlin, Heidelberg, pp. 1–46.
682 https://doi.org/10.1007/10_2017_16

683 Kracke, F., Lai, B., Yu, S., Krömer, J.O., 2018. Balancing cellular redox metabolism in microbial
684 electrosynthesis and electro fermentation – A chance for metabolic engineering. Metab Eng.
685 https://doi.org/10.1016/j.ymben.2017.12.003

686 Krieg, Thomas, Madjarov, Joana, Rosa, Luis F M, Enzmann, Franziska, Harnisch, Falk, Holtmann, Dirk,
687 Rabaey, Korneel, Krieg, T, Enzmann, F, Holtmann, D, Madjarov, J, Rosa, L F M, Harnisch, F,
688 Rabaey, K, 2018a. Reactors for Microbial Electrobiotechnology. Adv Biochem Eng Biotechnol
689 167, 231–271. https://doi.org/10.1007/10_2017_40

690 Krieg, T., Phan, L.M.P., Wood, J.A., Sydow, A., Vassilev, I., Krömer, J.O., Mangold, K.M., Holtmann, D.,
691 2018b. Characterization of a membrane-separated and a membrane-less electrobioreactor for
692 bioelectrochemical syntheses. Biotechnol Bioeng 115, 1705–1716.
693 https://doi.org/10.1002/BIT.26600

694 Lieder, M., Rashid, A., 2016. Towards circular economy implementation: A comprehensive review in
695 context of manufacturing industry. J Clean Prod 115, 36–51.
696 https://doi.org/10.1016/j.jclepro.2015.12.042

697 Logan, B.E., Rossi, R., Ragab, A., Saikaly, P.E., 2019. Electroactive microorganisms in
698 bioelectrochemical systems. Nat Rev Microbiol. https://doi.org/10.1038/s41579-019-0173-x

699 Nevin, K.P., Woodard, T.L., Franks, A.E., Summers, Z.M., Lovley, D.R., 2010. Microbial
700 electrosynthesis: Feeding microbes electricity to convert carbon dioxide and water to
701 multicarbon extracellular organic compounds. mBio 1, e00103-10.
702 https://doi.org/10.1128/mBio.00103-10

Pillot, G., Sunny, S., Comes, V., Heussner, A., Kerzenmacher, S., 2022a. Effect of cathode properties on the thermophilic electrosynthesis of PolyHydroxyAlkanoates by *Kyrpidia spormannii*. Bioresour Technol Rep 18, 101040. https://doi.org/10.1016/J.BITEB.2022.101040

Pillot, G., Sunny, S., Comes, V., Kerzenmacher, S., 2022b. Optimization of growth and electrosynthesis of PolyHydroxyAlkanoates by the thermophilic bacterium *Kyrpidia spormannii*. Bioresour Technol Rep 17, 100949. https://doi.org/10.1016/J.BITEB.2022.100949

Prévoteau, A., Carvajal-Arroyo, J.M., Ganigué, R., Rabaey, K., 2020. Microbial electrosynthesis from $CO_2$: forever a promise? Curr Opin Biotechnol. https://doi.org/10.1016/j.copbio.2019.08.014

Reiner, J.E., Geiger, K., Hackbarth, M., Fink, M., Lapp, C.J., Jung, T., Dötsch, A., Hügler, M., Wagner, M., Hille-Reichel, A., Wilcke, W., Kerzenmacher, S., Horn, H., Gescher, J., 2020. From an extremophilic community to an electroautotrophic production strain: identifying a novel Knallgas bacterium as cathodic biofilm biocatalyst. ISME J 14, 1125–1140. https://doi.org/10.1038/S41396-020-0595-5

Reiner, J.E., Jung, T., Lapp, C.J., Siedler, M., Bunk, B., Overmann, J., Gescher, J., 2018a. *Kyrpidia spormannii* sp. nov., a thermophilic, hydrogenoxidizing, facultative autotroph, isolated from hydrothermal systems at São Miguel Island, and emended description of the genus *Kyrpidia*. Int J Syst Evol Microbiol 68, 3735–3740. https://doi.org/10.1099/IJSEM.0.003037/CITE/REFWORKS

Reiner, J.E., Lapp, C.J., Bunk, B., Spröer, C., Overmann, J., Gescher, J., 2018b. Complete Genome Sequence of *Kyrpidia* sp. Strain EA-1, a Thermophilic Knallgas Bacterium, Isolated from the Azores. Genome Announc 6, e01505-17. https://doi.org/10.1128/genomeA.01505-17

Rodziewicz, J., Mielcarek, A., Janczukowicz, W., Jóźwiak, T., Struk – Sokołowska, J., Bryszewski, K., 2019. The share of electrochemical reduction, hydrogenotrophic and heterotrophic denitrification in nitrogen removal in rotating electrobiological contactor (REBC) treating wastewater from soilless cultivation systems. Science of The Total Environment 683, 21–28. https://doi.org/10.1016/J.SCITOTENV.2019.05.239

728 Sayess, R.R., Saikaly, P.E., El-Fadel, M., Li, D., Semerjian, L., 2013. Reactor performance in terms of
729 COD and nitrogen removal and bacterial community structure of a three-stage rotating
730 bioelectrochemical contactor. Water Res 47, 881–894.
731 https://doi.org/10.1016/J.WATRES.2012.11.023

732 Utesch, T., Zeng, A.P., 2018. A novel All-in-One electrolysis electrode and bioreactor enable better
733 study of electrochemical effects and electricity-aided bioprocesses. Eng Life Sci 18, 600.
734 https://doi.org/10.1002/ELSC.201700198

735 van den Berg, L., Kirkland, C.M., Seymour, J.D., Codd, S.L., van Loosdrecht, M.C.M., de Kreuk, M.K.,
736 2020. Heterogeneous diffusion in aerobic granular sludge. Biotechnol Bioeng 117, 3809.
737 https://doi.org/10.1002/BIT.27522

738 Vassilev, I., Dessì, P., Puig, S., Kokko, M., 2022. Cathodic biofilms – A prerequisite for microbial
739 electrosynthesis. Bioresour Technol. https://doi.org/10.1016/j.biortech.2022.126788

740 Wagner, M., Horn, H., 2017. Optical coherence tomography in biofilm research: A comprehensive
741 review. Biotechnol Bioeng 114, 1386–1402. https://doi.org/10.1002/BIT.26283

742 Wood, J.C., Grové, J., Marcellin, E., Heffernan, J.K., Hu, S., Yuan, Z., Virdis, B., 2021. Strategies to
743 improve viability of a circular carbon bioeconomy-A techno-economic review of microbial
744 electrosynthesis and gas fermentation. Water Res 201.
745 https://doi.org/10.1016/J.WATRES.2021.117306

746 Zeppilli, M., Lai, A., Villano, M., Majone, M., 2016. Anion vs cation exchange membrane strongly
747 affect mechanisms and yield of $CO_2$ fixation in a microbial electrolysis cell. Chemical Engineering
748 Journal 304, 10–19. https://doi.org/10.1016/J.CEJ.2016.06.020

749 Zhang, S., Jiang, J., Wang, H., Li, F., Hua, T., Wang, W., 2021. A review of microbial electrosynthesis
750 applied to carbon dioxide capture and conversion: The basic principles, electrode materials, and
751 bioproducts. Journal of $CO_2$ Utilization. https://doi.org/10.1016/j.jcou.2021.101640